We were awarded 15 shifts on ID27 to study the melting behaviour of Fe-Ni alloys, relevant to Earth's core, at high pressure in the laser heated diamond anvil cell. This beam-time was initially split into two sessions: six shifts in September 2012 and nine shifts in February 2013. A technical problem occurred on the beam-line during the second session, preventing accurate temperature measurement, which could not be resolved, in spite of the unwavering efforts of the beam-line staff. This necessitated a switch to alternative, room temperature experiments, unrelated to the original proposal, which were nevertheless very successful. As a result of this problem, we were awarded a further nine shifts in May 2013. Below are listed the experimental results achieved during these three sessions:

1. The melting curve of pure Ni

Our first aim was to measure the melting curve of the pure Ni end member in the Fe-Ni binary system. We determined the melting curve of Ni to 125 GPa using two complementary melting criteria: Firstly, the appearance of liquid diffuse scattering (LDS) during *in situ* XRD at ID27 and secondly, plateaux in temperature vs. laser power functions in both the *in situ* experiments and off-line experiments performed at our home lab in Bristol (Fig. 1). Our new melting curve is in good agreement with the majority of the theoretical studies on Ni melting and matches exactly the available shock wave melting data. It is however dramatically steeper than the previous off-line LH-DAC studies in which melting was based on the visual observation of motion aided by the laser speckle method. On the basis of these results we estimate the melting point of Ni at the inner-core boundary (ICB) pressure of 330 GPa as 5900 K, close to the value for pure Fe of 6200 K determined in a recent *in situ* LH-DAC study, also performed at ID27 which used similar methods to those employed here [10]. This similarity suggests that the alloying of 5-10 wt.% Ni with the Fe-rich core alloy is unlikely to have a significant effect on the temperature of the ICB, though this does depend on the topology of the Fe-Ni phase diagram. This value is however ~3300 K higher than the value determined on the basis of the earlier LH-DAC studies employing the laser speckle method. We find that those earlier melting curves coincide with the onset of rapid sub-solidus recrystallization, suggesting that visual observations of melt motion may misinterpret recrystallization as melting. This finding has significant implications for our understanding of the high-pressure melting behaviour of a number of other transition metals.

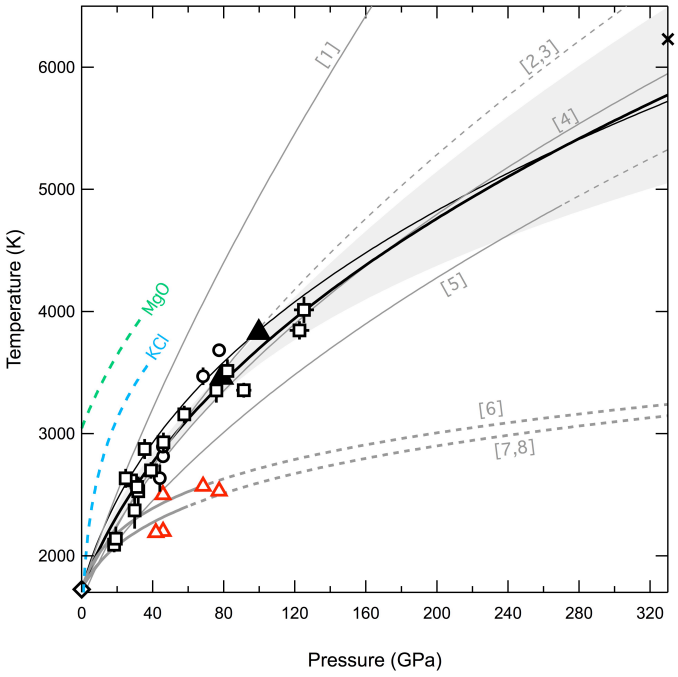

Figure 1 | Ni melting data collected *in situ* at the ESRF (circles) and off-line at Bristol (squares). For clarity, only the data corrected for the effects of thermal pressure are shown. The thick black line is an equally weighted fit using the Simon-Glatzel equation while the grey field is a 2σ error envelope. The thin black line is a similar fit to the uncorrected data (not shown). The red open triangles represent the estimated temperature of the onset of rapid recrystallization in our *in situ* experiments. The grey lines represent other Ni melting curves reported in the literature based on experiments (thick) and MD simulations (thin) with dashed lines representing extrapolation. Closed triangles: shock melting points recalculated by [2] on the basis of the equations of state of liquid and solid Ni reported by [9]. The black cross at 330 GPa represents the melting point of pure Fe based on the *in situ* experiments of [10]. Experimentally determined melting curves for the MgO and KCl pressure media are from [20] and [21] respectively.

Lord, O. T. et al. (2014). The melting curve of Ni to 1 Mbar. Earth and Planetary Science Letters, 408, 226–236. doi:10.1016/j.epsl.2014.09.046

2. The phase diagram of NiSi

Our original motivation for studying the melting curves of Fe-Ni alloys was based on the dramatic disagreement between the existing experimental melting curves of Ni and Fe, which suggested that the alloying of Ni with Fe in the inner core would significantly reduce the melting temperature of the Fe-rich core alloy and thus the temperature at the ICB. Our new *in situ* Ni melting curve, which agrees closely with that of Fe, overturns this hypothesis, thus making our planned study of the melting curves of the intermediate Fe-Ni alloys of less importance. In light of this result, we decided to change our strategy and study the phase diagram of NiSi instead.

Our interest in NiSi stems from its position as an end-member compound in the Fe-Ni-Si system, which has a great deal of relevance to the cores of the terrestrial planets. Geochemical models of the Earth based on cosmochemical arguments suggest that the Earth's core could contain at least 5 wt.% nickel [11] and up to 20 wt.% silicon [11,12]. As a result, several studies have been published concerning the sub-solidus phase relations [13] and melting behaviour [14] of a range of ternary alloys within the Fe-Ni-Si system. Recently, we began an ongoing effort to study the NiSi end-member, the behaviour of which was entirely unknown at the high-pressure, high-temperature conditions relevant to the interior of the Earth. Our primary motivation for studying the NiSi phase diagram is to provide vital data for those involved in continuing efforts to produce accurate thermodynamic descriptions of core liquids. Additionally, we wanted to determine the effects of Ni on FeSi at the conditions of Earth's core mantle boundary (CMB) region where solid B2 structured FeSi may well be present. All pathways for the formation of FeSi involve the iron-rich alloy of the underlying core, and so, given the expected solid solution between the isostructural NiSi and FeSi phases, we would expect any silicide present to be iron-rich (Fe,Ni)Si in the B2 structure [15]. Knowledge of the phase diagram of NiSi will

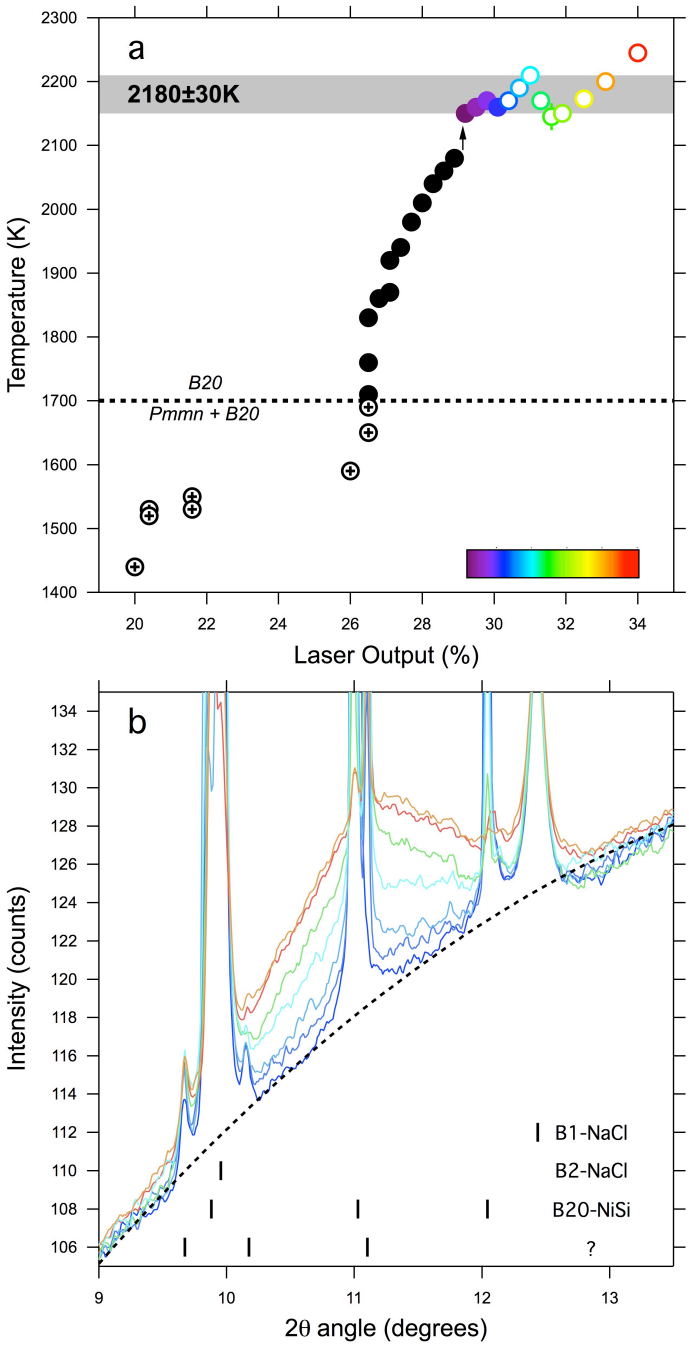

Figure 2 | (a) Temperature vs. laser power plot. Open circles with plus sign: *Pmmn* + B20 phases present in XRD patterns; Solid black circles: B20-NiSi. The dashed line represents the temperature above which the *Pmmn* phase was no longer observed and the grey bar represents the melting temperature determined from the points within the melting plateau, which are colour coded as a function of laser output. The open circles represent XRD patterns in which LDS was observed. (b) XRD patterns colour coded to match (a). The black dashed line represents the background fit to the pattern collected immediately before LDS was observed. Tick marks from top to bottom represent B1-NaCl, B2-NaCl, B20-NiSi and an unidentified trace phase.

give additional constraints on the stability of this material within the CMB region.

We determined the sub solidus phase diagram and melting curve of NiSi to 70 GPa using the same methods and melting criteria employed for our study of pure Ni. Fig. 2 shows an example of the melting data acquired *in situ* at ID27. Our results confirm that any (Fe,Ni)Si phase present within the Earth's CMB region will have the B2 structure, and that it will remain as a stable solid, except in the hottest regions immediately adjacent to the core.

Published as: Lord, O. T. et al. (2014) The NiSi melting curve to 70 GPa. Phys. Earth Planet. Inter. 233, 13-23.

Published as: Dobson, D. P. et. al. (In Press) The phase diagram of NiSi under the conditions of small planetary interiors. Phys. Earth Planet. Inter.

3. The equation of state of perovskite (Pv) and post-perovskite (PPv) structured $NaCoF_3$

During our second session in February 2013, when laser-heating experiments were not possible due to a technical problem on the beamline, we took the opportunity to perform a room temperature compression experiment on $NaCoF_3$ in a membrane driven cell, using Ne as the pressure medium.

The lower mantle of the Earth is comprised mainly (~70 vol%) of minerals with the general stoichiometry (Mg,Fe)(Al,Si)O3: at pressures below 120 GPa this takes the orthorhombic Pv structure and above 120 GPa the CaIrO3 PPv structure. This PPv phase has received considerable interest since its discovery since its elastic [e.g. 16] and transport properties [e.g. 17] seem to explain many of the seismic anomalies which have been detected in the D'' region of the lowermost mantle. Unfortunately, due to its high stabilization pressure, many of the properties of interest are not directly measurable in MgSiO3 PPv and so a combination of atomistic simulation and experiment on low-pressure analogues has proven fruitful in predicting the properties of the D'' region. $NaCoF_3$ is such an analogue material that shows great promise [18]. Furthermore, a recent study [19] predicted that NaMgF3 PPv would transform to new, denser, structures at pressures above 60 GPa and 210 GPa, which we term P2Pv and P3Pv respectively; similar high-pressure transitions might occur in MgSiO3 in the TPa region relevant to super-Earths.

During our compression experiment at ID27, not only did we determine the equation of state of both the Pv and PPv structured polymorphs of $NaCoF_3$ we also detected the P2Pv phase at 23 GPa, which persisted to the highest pressure reached (65 GPa) before back-transforming to PPv on decompression. This is the first time that this structure has been detected in any material.

A paper describing these results is currently in preparation.

4. The equation of state of *Pmmn* structured NiSi

Also during our second session, we performed a compression experiment on the recently discovered [22] *Pmmn* structured polymorph of NiSi. This phase is expected to be stable at pressures above ~12 GPa and temperatures below ~1200 K [23] and thus may be a relevant end-member in the multi-component system describing the cores of small planetary bodies. As with the $NaCoF_3$ sample, we compressed the NiSi sample in a membrane driven cell, using Ne as the pressure medium.

The resulting lattice parameters are in excellent agreement with those of *ab initio* simulations reported in a recent study, as are the resulting equation of state parameters [22].

Published as: Lord, O. T. et al. (2015) The equation of state of the Pmmn phase of NiSi. J. App. Cryst. 48, 6, 1914-1920

5. Phase relations of sediments at the CMB

Finally, we performed a pair of *in situ* XRD experiments at CMB conditions (130 GPa, 2500 K) to determine the phase relations of two model silicate compositions representing oceanic sediments (clays) subducted into the deep mantle and the restite (or residuum) expected to remain after melting of the clay composition in the upper mantle. These data have now been analysed, and suggest that at CMB conditions, the clay composition forms an assemblage of Seifertite + calcium ferrite (CF) structured phase while the restite forms the assemblage Seifertite + CF + Mg-Pv (± Ca-Pv). These results are in good agreement with previous off-line LH-DAC and multi-anvil press experiments already performed by us and will allow us to determine the evolution of the phase relations of subducted sediments throughout the whole of Earth's mantle.

A paper describing these results is currently in preparation.

References: [1] Luo, F. et al. (2010) J Chem Eng Data 55:5149-5155; [2] Pozzo M & Alfè D (2013) Phys Rev B 88:024111; [3] Weingarten, N.S. et al., Mattson WD, Rice BM (2009) J App Phys 106:063524; [4] Koči, L. et al. (2006) Phys Rev B 74:012101; [5] Bhattacharya, C. et al. (2011) Physica B 406:4035-4040; [6] Lazor, P. (1993) Phys Chem Minerals 20:86-90; [7] Errandonea, D. (2013) Phys Rev B 87:054108; [8] Japel, S. et al. (2005) Phys Rev Lett 95:167801; [9] Urlin, V. D. (1966) Soviet Phys JETP 22:341; [10] Anzellini, S. et al. (2013) Science 340:464-466; [11] Allègre, C. J. (1995) Earth Planet Sci Lett 134:515-526; [12] Fischer, R. A. (2012) Earth Planet Sci Lett 357–358:268–276; [13] Sakai, T. (2011) Geophys Res Lett 38:L09302; [14] Morard, G. et al. (2011) Phys Chem Minerals 38:767-776; [15] Lord, O.T. et al. (2012) J App Cryst 45:726-737; [16] Stackhouse, S. et al. (2005) Geophys. Res. Lett., 32, L13305; [17] Ammann, M.W. et al. (2011) Nature, 465, 462-465, 2010; [18] Dobson, D. P. et al. (2011) Phys. Earth. Planet. Inter., 189, 171-175; [19] Umemoto, K & Wentzcovitch, R.M. (20060 Phys. Rev. B 74, 224105. [20] Zerr, A., Boehler, R. (1994) Nature 371:506-508 [21] Boehler, R. (1996) Phys. Rev. B 53:556-563. [22] Wood, I. G. et al. (2013) J. App. Cryst. 46:14-24. [23] Dobson, D. P. et al. (under review) Phys. Earth Planet. Inter.